Nanoscale Calorimetry Using a Suspended Bridge Configuration

Shu Zhang, Yoed Rabin, Yizhang Yang, and Mehdi Asheghi

Abstract—A new setup for small-scale differential scanning calorimetry (DSC) studies based on a suspended bridge configuration is presented. The new setup has three major advantages over previously reported DSC setups: 1) superior temperature uniformity in the bridge cross section; 2) less heat loss to the surroundings by at least two orders of magnitude; and 3) a faster transient response by three orders of magnitude. This paper includes a thermal analysis to support these improvements. A major contribution of the new thermal analysis over previous reports is the inclusion of the thermal mass of the substrate in calculations, which makes thermal design more detailed, dramatically affecting accuracy and sensitivity in measurements. Furthermore, the new thermal analysis more accurately accounts for heat loss to the substrate and the surroundings in efforts to resolve suspected inconsistencies in previously reported data. Experimental validation of the new setup is presented by measuring the specific heat of thin layers of SiO_2 and CoFe. The specific heat of SiO_2 was found to be 2.2×10^6 Jm^{-3} K^{-1}, which is nearly 10% different from the literature values of bulk specimens. For CoFe, the specific heat value of 3.16×10^6 Jm^{-3} K^{-1} is obtained using differential Cu/SiO_2 and $Cu/SiO_2/CoFe$ structures compared to the value of 3.5×10^6 Jm^{-3} K^{-1} obtained using single CoFe suspended structure. **[1449]**

Index Terms—Differential scanning calorimetry (DSC), frequency domain, nanocalorimetry, suspended bridge, thermal analysis, time domain.

I. INTRODUCTION

CALORIMETRY is the process of quantifying internal energy changes as a result of temperature changes, in which the measure of the internal energy is the thermophysical property of enthalpy. In a single-phase process, changes in internal energy are associated with temperature changes (sensible heat), and the amount of energy required to elevate the temperature of the material in one degree of temperature is known as the thermophysical property of specific heat. When the temperature of the material exceeds the phase transition temperature, additional energy is required to rearrange the bonds between the molecules of the material. In a pure material, this energy change is not associated with a change in temperature and is known as the thermophysical property of latent heat. In a non-pure material, in which rearrangement of molecular bonds may take place sequentially over a temperature range, the distinction between sensible heat and latent heat is not easy to establish, and the combined effect is typically measured. The rate at which internal energy changes can take place in a non-pure material is bounded by many factors, and the analysis of the kinetics of such a process is quite challenging.

The increasing need to quantify internal energy changes on a small scale—whether in the form of sensible heat or in the form of latent heat—motivated the current study [1]–[3]. Over the past few years, the need for small-scale measurements led to the development of small-scale calorimetric techniques, which are primarily based on electrical resistance heating and thermometry. The related small-scale calorimetric setups typically have the configuration of a patterned bridge sensor on a suspended substrate, which allows for low-power and high-sensitivity measurements (on the order of 100–1000 nJ). Reports on such techniques include measurements of enthalpy changes associated with phase transition, melting point depression, reduction of melting enthalpy, abnormal discontinuities in the heat of melting for small particles in the range of 2–5 nm [4]–[9], and specific heat measurement for samples in the range of 3–5 μg [10], [11]. While the above reports revealed novel phenomena associated with small-scale heat transfer, simplified thermal design of early sensors and techniques affected the quality of measurements. More specifically, the thermal mass of the substrate has been neglected in thermal analyses of the previous setups, which dramatically affected the accuracy and sensitivity of measurements. Furthermore, simplified thermal analysis of heat loss from the substrate to the surroundings affected measurements and may have been one of the key sources for inconsistencies in previously reported data. Tai *et al.* [17] and Arx *et al.* [20] used microbridges to measure the thermal conductivity of heavily doped polycrystalline silicon films and the thermal conductance and heat capacitance of complementary metal–oxide–semiconductor integrated circuit layer sandwiches, respectively, which lead to a more uniform temperature distribution within the bridge cross section and a better approximation of the bridge as a lumped system.

In this paper, an improved thermal analysis of a previously reported small-scale calorimetric setup [9] is proposed. This analysis reveals the motivation in developing an improved calorimetric technique for small-scale studies. Next, a new setup for small-scale calorimetry is presented based on a suspended bridge configuration. The new technique is based on data analysis in both time and frequency domains. Finally, a
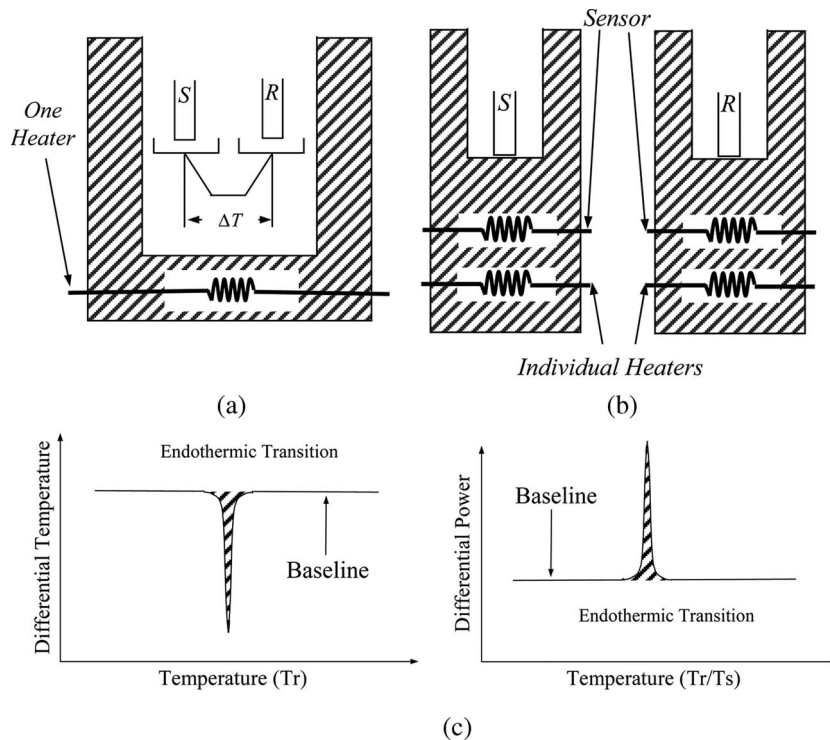
Fig. 1.   Schematic illustration of devices for (a) DTA, (b) DSC, and (c) typical output during DTA and DSC experiments.

validation test is carried out and presented on Cu, SiO$_2$, and CoFe, which have been used extensively in semiconductor and data storage applications.

II. PRIOR ART: DIFFERENTIAL SCANNING CALORIMETRY (DSC) AND DIFFERENTIAL THERMAL ANALYSIS (DTA) TECHNIQUES

The most commonly used calorimetry techniques are DSC and DTA, as illustrated in Fig. 1. In DTA, a single heater is used to elevate both the temperature of a measured sample T_S and the temperature of a reference specimen T_R while the temperature difference between the sample and the reference $T_S - T_R$ is measured continually. By contrast, two independent heaters are used in DSC in order to elevate the temperature of the sample and the reference. Using a closed-loop control system, the power on each of the DSC heaters is controlled in order to maintain the same temperature in the sample and the reference $T_S = T_R$, while the power difference between the heaters is continually recorded $P_S - P_R$. Fig. 1(c) shows typical output from the DTA and DSC setup. Note that the DTA curve is similar to an inverted DSC curve. The baseline value shown in Fig. 1(c) corresponds to the difference in the thermal properties between the sample and the reference. The sudden change of the output signal from its baseline value corresponds to a sudden change in internal energy of the sample, possibly related to phase transition.

Lai *et al.* [12], [13] introduced a new generation of small-scale DSC devices, which use two identical electrical resistance heating/thermometry patterned metallic bridges on a suspended membrane [Fig. 2(a)]. This microstructure consists of a 100-nm-thick amorphous Si–N suspended membrane and two thin-film Ni bridges deposited on top of the membrane. Both bridges have identical dimensions: effective length of 8 mm, thickness of 30 nm, and width of 0.4 mm. The combination of overlying layers allowed each bridge to serve as both a heater and a thermometer. A thin Sn layer was deposited on the opposite side of the membrane using a shadow mask, which has approximately the same width and length as the Ni heater, and a thickness of 1 nm. The bridge at the vicinity of the Sn layer together with the Sn layer was defined as the "sample structure," while the other bridge was defined as the "reference structure."

Measurements were performed by applying a current pulse to the metal bridges while recording the resulting voltage versus current on the bridge. The power input to the reference structure and the sample structure was calculated as the product of the measured voltage and current. The resistance of the bridge was calculated as the ratio of voltage-to-current, and the bridge temperature was calculated from a calibration curve of electrical resistance as a function of temperature, which was prepared in advance. As illustrated in Fig. 2(b), the reference voltage V_R continually increases with time due to the increase in electrical resistance with the increase in temperature. The sample voltage V_S responded slower in comparison with the reference voltage due to the additional thermal mass of the Sn sample. The constant voltage output segment—between 6 and 8.5 ms in Fig. 2(b)—is likely to correspond to the melting process of the Sn sample. During Sn melting, internal energy changes associated with the latent heat effect overwhelm internal energy changes associated with the sensible heat effect.

Lai *et al.* [12], [13] applied the following underlying assumptions in their data analysis: 1) heat losses to the surrounding are negligible and 2) although constructed on a membrane, the bridge specimen structure can be approximated as a lumped

This article has been accepted for inclusion in a future issue of this journal. Content is final as presented, with the exception of pagination.

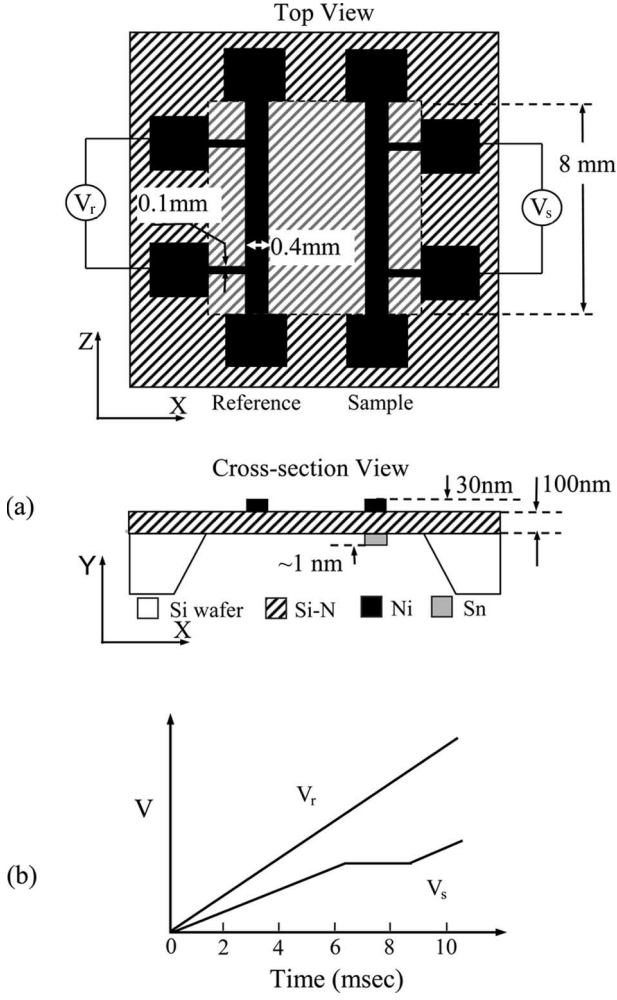ZHANG *et al.*: NANOSCALE CALORIMETRY USING A SUSPENDED BRIDGE CONFIGURATION 3

Fig. 2. Schematic illustration of (a) membrane-based microcalorimeter [12], [13] and (b) typical voltage output during phase change.

system. Under these assumptions, the sensible heat can be calculated from an energy balance on a lumped system

$$P = IV = wblC_p \frac{dT}{dt} \qquad (1)$$

where w, b, and l are the width, thickness, and length of the lumped system, respectively, C_p is the specific heat, and t is time. Further assuming that the specific heat is constant, (1) can be rewritten in a more practical form for data analysis

$$\int_{t_O}^{t} P \, dt = wblC_p(T - T_O) \qquad (2)$$

where T_O is the temperature at initiation of the experiment at time t_O.

Finally, when a change in internal energy occurs as a result of a phase change process, the sensible heat term can be substituted with a latent heat term as

$$\int_{t_O}^{t} P \, dt = wblH \qquad (3)$$

where H is the latent heat. For a non-pure material—as is the case in many small-scale experiments—latent heat is released over a temperature interval known as the phase transition temperature range. Hence, (1) is commonly used for phase transition processes as well, but then the term "effective specific heat" is used instead of the intrinsic property of specific heat. The dynamics of phase transition is a function of many factors, such as the heating rate and the typical dimensions of the structure [4], [5]. The technique presented above is also applicable to thin films of liquids [6]–[9].

III. THERMAL ANALYSIS OF PRIOR ART

With reference to Fig. 2, three typical dimensions characterize heat transfer on the membrane suspended sensor: w, b, and l in the x, y, and z directions. With respect to heat transfer in the y-direction, the Biot number is defined as

$$\text{Biot} = \frac{bU}{k} \qquad (4)$$

where k is the thermal conductivity, and U is the overall heat transfer coefficient to the surroundings, which combines radiation and convection effects. A typical Biot number for the calorimetric setup is less than 10^{-7}, where the typical membrane thickness is on the order of 100 nm, the typical thermal conductivity is on the order of 1–100 W/m-K, and the typical heat transfer coefficient value is 15 W/m^2-K. This low Biot number indicates that the bridge–membrane system can be lumped in the y direction, and as a result, the following analysis addresses temperature distribution in the x and z directions only.

Since l is typically an order of magnitude longer than w, and in order to estimate the temperature distribution in the x-direction at the center of the sensor–membrane setup, this setup can be approximated as infinite in the z direction for the purpose of the current analysis. Under these conditions, the heat transfer problem in the x direction can be presented as

$$\frac{1}{\alpha}\frac{\partial T}{\partial t} = \frac{\partial^2 T}{\partial x^2} + \frac{q}{k}; \quad q = \begin{cases} q_o, & 0 \le x < w/2 \\ 0, & w/2 \le x < \infty \end{cases} \qquad (5)$$

where k and α are the lumped properties of thermal conductivity and thermal diffusivity in the y direction, respectively, and q_o is the volumetric heat generation in the bridge.

The solution of (5) for the elevated temperature in an infinite domain, assuming a uniform initial temperature, is recompiled from Carslaw and Jaeger [14]:

$$\varphi = \begin{cases} 1 - 2i^2\text{erfc}\left(\frac{1-\xi}{2\sqrt{Fo_y}}\right) - 2i^2\text{erfc}\left(\frac{1+\xi}{2\sqrt{Fo_y}}\right), & 0 \le \xi < 1 \\ 2i^2\text{erfc}\left(\frac{\xi-1}{2\sqrt{Fo_y}}\right) - 2i^2\text{erfc}\left(\frac{\xi+1}{2\sqrt{Fo_y}}\right), & 1 \le \xi < \infty \end{cases} \qquad (6)$$

We use the following dimensionless numbers:

$$Fo_y = \frac{\alpha t}{(w/2)^2}, \quad \varphi = \frac{T}{Fo_y A_O}, \quad A_O = \frac{q_o w^2}{4k}, \quad \xi = \frac{x}{w/2} \qquad (7)$$

This article has been accepted for inclusion in a future issue of this journal. Content is final as presented, with the exception of pagination.

4   JOURNAL OF MICROELECTROMECHANICAL SYSTEMS
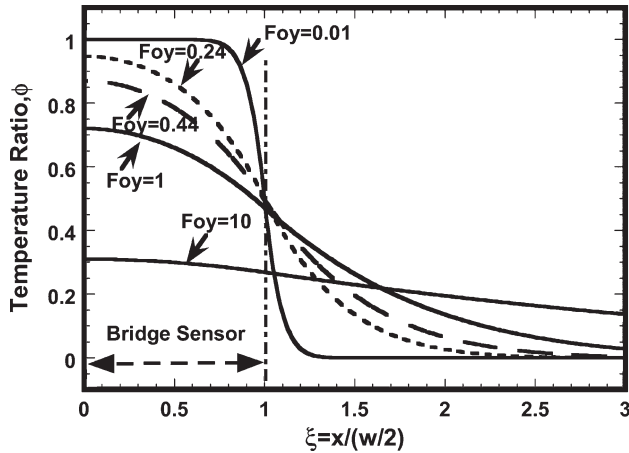

Fig. 3.   Temperature ratio φ (6) representing the deviation of the temperature distribution across the sensor bridge from a uniform value; $\varphi = 1$ everywhere for a lumped system.

where

$$i^2\mathrm{erfc}(\gamma) = \frac{1}{4}\left[(1+2\gamma^2)\mathrm{erfc}(\gamma) - \frac{2}{\sqrt{\pi}}\gamma\exp(-\gamma^2)\right] \quad (8)$$

and where γ is a dummy variable. Note that the product of $Fo_y A_O$ is the elevated temperature if the sensor–membrane couple could indeed be considered as a lumped system. Therefore, the parameter φ represents the ratio of the actual temperature elevation to the elevated temperature that would develop in the system if the system could be considered lumped.

The temperature ratio φ is a function of the dimensionless location ξ and the dimensionless time Fo_y, which is also known as the Fourier number. In the thermal sense, a process characterized by a small Fourier number ($\ll 1$) is known to be at its initiation, while a process characterized by a large Fourier number ($1 \ll$) is approaching a steady state. For example, the sensor–membrane setup described by Efremov et al. [9] has a width of 0.5 mm, a typical duration of experiment of up to 8 ms, and the Fourier number for the system described there has a range of 0.24–0.44 with the thermal diffusivity reported by Zhang and Grigouopoulos [15].

Fig. 3 presents the temperature ratio φ as a function of the dimensionless location ξ for various Fo_y values, as calculated from (6). The average temperature ratio value in the range of $0 \leq \xi < 1$ is 0.962, 0.816, 0.752, 0.638, and 0.296 for Fo_y values of 0.01, 0.24, 0.44, 1, and 10, respectively. It follows that for the experimental conditions reported by Efremov et al. [9] (dash line), for example, the average elevated temperature in the sensor after 8 ms of experimentation is only 75%–82% of its expected elevation if it indisputably behaved like a lumped system; this leads to an 18%–25% error in specific heat estimation in this particular example. The effect of the heater's diffusivity is neglected in this discussion when the heater's thickness is negligible compared with the membrane's thickness; for the case where the heater's thickness is comparable with the membrane's thickness, the temperature profile within the metal strip will be flatter because of the metal strip's higher thermal

conductivity, which will leads higher Fo_y values—the cost for the more uniform temperature profile is that the heat loss through the membrane will increase since the energy for the control volume is conserved.

The DSC setup reads the difference between the reference bridge and the sample bridge, which will reduce but not completely cancel out the error introduced by heat loss through the membrane. The reason is that the effect of adding the specimen on the sample bridge will be distributed in a similar manner to the effect of the bridge–membrane couple as discussed above, which will make the heat loss through the membrane to be different for the sample bridge and the reference bridge. The result is verified by ANSYS finite-element simulations. With setting value of 4.3×10^8 J/m^3, the average temperature of the metal strip is obtained by averaging the element temperature under that area, and the latent heat of Sn is calculated as 4.74×10^8 J/m^3 with the method reported by Efremov et al. [9], which represents 10.2% error.

In this regard, it could be argued that the DSC setup reads the difference between the reference bridge and the sample bridge, and therefore the lumped system assumption is not critical for the analysis. However, the effect of adding the specimen on the sample bridge will be distributed in a similar manner to the effect of the bridge–membrane couple, as discussed above. While the DSC concept is set to capture differences between similar bridges, data analysis for obtaining thermophysical properties based on previous setups is not straightforward, and (1)–(3) cannot be used for this purpose.

The underlying assumption that the sensor is infinitely long in the z direction was made here in order to simplify the mathematical analysis and the solution in (6). However, this simplification leads to the best-case scenario, while the actual 2-D nature of the heat transfer process on the membrane surface will reduce the maximum temperature for any given Fo_y number; this will also increase the magnitude of temperature distribution on the membrane surface. Hence, further 2-D or 3-D thermal analysis is not deemed to be useful.

It can be concluded that the temperature distribution in the setup presented by Efremov et al. [9] can by no means be considered uniform, which makes the lumped system assumption questionable. At least two alternatives are available to correct this technical problem: improving the data analysis technique (which is expected to become very cumbersome) or redesigning the sensor–substrate setup, which is the subject matter of the current report.

IV. New DSC Setup

The design concept applied for the development of the new setup is that the sensor must be, as much as possible, thermally insulated from the substrate, which led to a suspended bridge configuration [17], [20]. This is expected to lead to a more uniform temperature distribution within the bridge cross section and a better approximation of the bridge as a lumped system, as discussed above. This configuration can also increase measurement sensitivity, as discussed below. The design and construction of the new DSC setup was performed at the Carnegie Mellon Nanofabrication Facility.
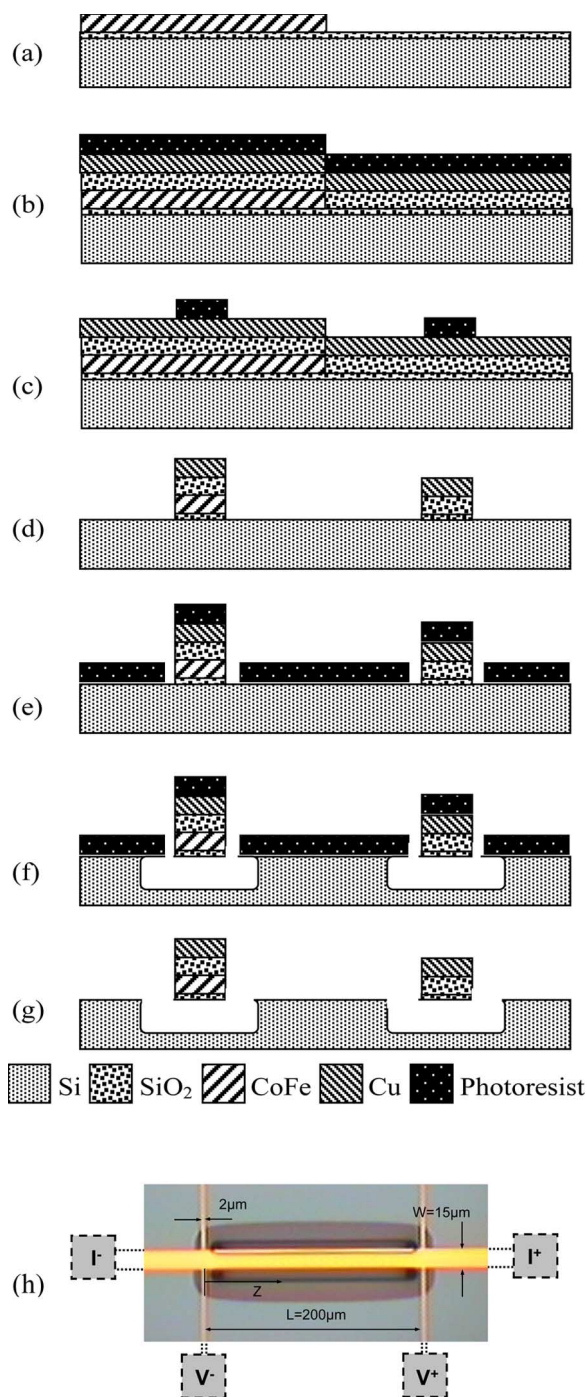
Fig. 4. Schematic of the bridge–substrate setup at various stages of fabrication. (a) CoFe is sputtered on half of the Si substrate. (b) SiO$_2$ and Cu layers are sputtered on top of the entire wafer and then spin photoresist on top. (c) Photoresist layer was patterned by Geophysis Corporation of America (GCA) stepper and developed. (d) Sections of CoFe, SiO$_2$, and Cu are removed by ion milling, and the photoresist is removed by acetone rinse. (e) Photoresist is spun and patterned to form trenches beside the bridges. (f) SF$_6$ plasma etches Si through the trenches to suspend the bridges. (g) Photoresist is removed by oxygen plasma etch. (h) Photo of the fabricated bridge.

Schematic illustrations of the fabrication process, and a photo of the sensor, are shown in Fig. 4. The fabrication process included the following steps.

1) The fabrication starts with the deposition of 144-nm-thick CoFe on top of a Si substrate coated with 10-nm-thick thermally grown SiO$_2$ layer. Only one-half of the Si substrate is covered with the CoFe layer by using a shadow mask during the sputter process [Fig. 4(a)].

2) A 105-nm-thick layer of SiO$_2$ and a 144-nm-thick layer of Cu are successively sputtered over the entire substrate. Next, a photoresist layer, with a thickness of about 1 μm, is spun [Fig. 4(b)].

3) A standard lithography process is performed with a GCA stepper to pattern the photoresist layer, which is later used as the protecting mask in the ion milling step that follows [Fig. 4(c)].

4) The pattern is copied from the photoresist layer to the structure layer (CoFe/SiO$_2$/Cu) by a 10-min ion mill etching application. Following the ion milling, the photoresist layer is removed by an acetone rinse [Fig. 4(d)].

5) A second lithography is processed to produce trenches, which are used for access in the next plasma etching step. With careful alignment control, the trenches are precisely positioned so that each metal strip is located between two trenches [Fig. 4(e)].

6) SF$_6$ plasma is used to etch the Si under the metal bridge through the trenches produced in Step 5). The SF$_6$ plasma has high selectivity between the Si substrate and the metal layer ($>100:1$) and is used to ensure that the metal bridge can be suspended without damage [Fig. 4(f)].

7) In order to remove the photoresist layer and to protect the suspended bridge, an application of 30 min of oxygen plasma is chosen [Fig. 4(g)] (instead of the commonly applied acetone rinse for photoresist removal).

8) Finally, the sample is glued to a chip carrier and processed for wire bonding.

A microscopic photo of the suspended bridge is shown in Fig. 4(h). The bridge with the layer of CoFe is the sample bridge, and the bridge without the CoFe layer functions as the reference bridge [see also Fig. 2(a)]. The layer of SiO$_2$ is used as an electrical insulation layer between the Cu layer and the CoFe layer.

The most challenging aspect of the fabrication process is making the sample bridge and the reference bridge identical. In order to minimize the uncertainty introduced by fabrication, the dies (which include the sample bridge and the reference bridge) are designed to be close together on the same Si substrate. Note that the sputtering and lithography processes are the main uncertainties that are introduced by fabrication. The Cu layer and the SiO$_2$ layer are sputtered in CVC Connexion 6 Target Sputtering System with uniformity of better than 2% and in 8L 3 Target Sputtering Machine with uniformity of better than 5% over the 3″ Si substrate, respectively. The distance between the sample bridge and the reference bridge is roughly ∼15 mm, which leads to an uncertainty in the thickness of Cu of 0.4% and of SiO$_2$ of 1%. The reported uncertainty level was experimentally verified by using profilometer in thickness measurement after the sputtering process. The uncertainty in width introduced by lithography is estimated to be less than 0.1%. The resulting uncertainty in volume is ∼1.1% (the square root of the sum of the square uncertainties). For a typical temperature elevation of 10 K, typical bridge dimensions of

244 nm $\times$ 15 μm $\times$ 200 μm, and a typical specific heat value of 3.11×10^6 Jm^{-3} K^{-1} (see Section VII), the typical energy consumption by the bridge is 23 nJ, and the typical uncertainty in measurement due to uncertainty in the bridge volume is 0.253 nJ.

V. THERMAL ANALYSIS OF THE NEW DSC SETUP

The superiority of the new setup originates from its suspended bridge configuration, which adds a significant thermal barrier between the bridge and the underlying membrane. The thermal resistance to heat transfer by conduction is proportional to the thickness of the barrier but inversely proportional to the thermal conductivity of the barrier. Radiation effects also take place between the bridge and the substrate. For small temperature difference between walls, where the gap is transparent, and for maximal heat transfer between black walls, the effective heat transfer coefficient by radiation h_{rad} can be approximated from

$$
\begin{aligned}
q'' &= \sigma \left(T_1^4 - T_2^4 \right) \\
&= \sigma \left(T_1^2 + T_2^2 \right) (T_1 + T_2)(T_1 - T_2) \\
&= h_{\mathrm{rad}}(T_1 - T_2) \qquad (9)
\end{aligned}
$$

where σ is the Stefan–Boltzmann constant. For example, for maximum wall temperatures of 293 and 493 K [9], the effective heat transfer coefficient by radiation is 14.6 W/m^2-K, which leads to a thermal resistance to heat transfer by radiation of 0.068 m^2-K/W (the inverse of the heat transfer coefficient). The thermal conductivity of air under the vacuum condition of 5×10^{-4} torr is 4.3×10^{-6} W/m-K, which was calculated as one-third of the product of the volumetric specific heat, separation distance between the suspended bridge and the bottom of the silicon cavity, and the average molecular velocity [16]. It is noted that the mean free path in air under such vacuum conditions is longer than the fabricated bridge-to-wall distance, and that the bridge-to-wall distance is used as the modified mean free path in the calculation. The thermal resistance to heat transfer of 50 μm deep air gap is 11.5 m^2-K/W (the depth of the air gap divided by the thermal conductivity). In comparison, the resistance to heat transfer by the copper bridge is 2×10^{-7} m^2-K/W. It follows that radiation effects and air conduction at low pressures do not significantly decrease the thermal resistance between the suspended bridge and the substrate in the new setup.

Since thermal resistance to heat transfer by radiation is comparable to thermal resistance to heat transfer by gas conduction, because it has already been shown that the Biot number is very small in the y direction, and because the Biot number in the new setup is also very small in the x direction, a uniform temperature distribution can be achieved in the bridge cross section.

The discussion turns now to the transient response of the DSC setup. The transient response is related to the ability of the bridge to change its temperature as a result of internal energy changes in the specimen. The transient response of previous setups [4]–[9] is affected by the thermal mass of the

bridge as well as the thermal mass of the membrane. As can be concluded from Fig. 3, there is a thermally affected region in the membrane to which some of the heat is transferred from the bridge. As a first-order approximation, if it is assumed in the current analysis that all the materials involved have similar volumetric specific heat, then the transient response is directly proportional to the effective volume of the bridge–substrate couple. In previous setups (and as can be approximated from Fig. 3), the effective width of the setup is at least three times the width of the bridge, and the effective thickness (including the bridge and the substrate) can easily exceed ten times the thickness of the specimen. It follows that the effective volume (the thermally affected volume) in the previous setup is at least 30 times the volume of the specimen. However, in the suspended bridge setup, the width of the affected volume is the bridge width, and the affected thickness is the bridge thickness, which is about three times the specimen thickness. It follows that the effective volume of the new setup is an order of magnitude smaller than the affected volume of the previous setup if the bridges of both setups are identical. In practice, the width and thickness of the bridge in the new setup are significantly smaller than the previous setup. Of course, the current discussion concerns the affected volume and not the affected thermal mass (= volume $\times$ specific heat). However, while a detailed analysis of the thermal mass may lead to a better approximation of the transient response, it is not expected to affect the magnitude of the difference between the pervious and the new setup. Due to the smaller thermal mass (at least an order of magnitude) of the new setup and the two orders of magnitude higher thermal resistance between the bridge and the substrate in the new setup, the transient response of the new setup is expected to be three orders of magnitude faster than that of the previous setup.

In summary, the new setup of a suspended bridge has three major advantages over the prior setups discussed above: 1) higher temperature uniformity in the bridge cross section; 2) lower heat losses to the surroundings by at least two orders of magnitude; and 3) transient response that is three orders of magnitude faster. It can be farther concluded that data analysis for the previous DSC setup is significantly less accurate due to the neglect of heat loss to the surroundings, significant nonuniformities in temperature distribution, and ignoring the coupled thermal effect of the bridge and the substrate.

VI. DATA ANALYSIS OF THE NEW DSC SETUP

The method of data analysis with the new setup is based both on the time-domain approach, which uses a pulse heating technique, and on the frequency-domain approach, which utilizes the so-called "3ω" technique. The approach to the time-domain analysis is presented here to enable sensitivity analysis in the new setup, while the approach of frequency-domain analysis is applied for validation of the experimental setup.

A. Data Analysis in the Time Domain

The experiment begins ($t = 0$) by imposing a current pulse (a step-like function) of amplitude I on the Cu layer of the

sample bridge. As a result, the temperature of the entire sample bridge is warmed. Following the thermal analysis presented above, it can be assumed that all generated heat is conducted along the bridge structure to the substrate through the bridge ends. This assumption becomes stronger if the setup is placed in a vacuum chamber. The thermal process can be modeled as a 1-D heat conduction problem in a thermal fin, which is driven by a uniform volumetric heat generation. Neglecting surface heat loss by radiation and conduction, and following the same approach described in [17], the governing equation becomes

$$\frac{\partial^2 T}{\partial z^2} + \frac{I^2 R_0}{wblk}\left[1 + \alpha_{\mathrm{er}}(T - T_0)\right] = \frac{1}{\alpha_p}\frac{\partial T}{\partial t} \quad (10)$$

where k is the equivalent lateral thermal conductivity of the bridge, R_0 denotes the electrical resistance of the bridge, α_{er} is the temperature coefficient of the electrical resistance (TCR), and α_p is the equivalent thermal diffusivity of the bridge. The boundary conditions are given by

$$T(z = 0) = T_0, \quad T(z = l) = T_0 \quad (11)$$

and the initial condition is

$$T(t = 0) = T_0. \quad (12)$$

Heat loss from the surface by radiation is certainly important if the bridge is long and if the temperature difference between the bridge and the substrate is great. However, for simplicity, the discussion with regard to radiative heat transfer is delayed. We use the following parameters:

$$\theta = T - T_0, \quad \delta = \frac{I^2 R_0}{k(wbl)}, \quad m^2 = \delta\alpha_{\mathrm{er}}. \quad (13)$$

The governing equation, boundary conditions, and initial condition can be written as

$$\frac{\partial^2 \theta}{\partial z^2} + m^2\theta = \frac{1}{\alpha_p}\frac{\partial \theta}{\partial t} - \delta \quad (14)$$

$$\theta(z = 0) = 0; \quad \theta(z = l) = 0 \quad (15)$$

$$\theta(t = 0) = 0. \quad (16)$$

The solution of (14)–(16) is

$$\theta = \theta_{ss}(z) + \theta_{tr}(z, t) \quad (17)$$

$$\theta_{ss}(z) = \frac{\delta}{m^2}\left(\frac{\cos m(z - l/2)}{\cos(ml/2)} - 1\right) \quad (18)$$

$$\theta_{tr}(z, t) = e^{Fo_z(l/2)^2\delta\alpha_{\mathrm{er}}}\sum_1^\infty C_n \sin\left(\frac{n\pi z}{l}\right)e^{-\frac{Fo_z}{4}(n\pi)^2} \quad (19)$$
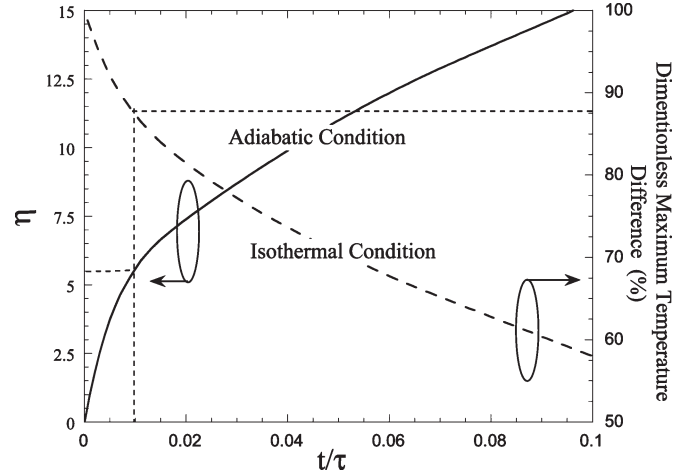

Fig. 5. Deviation from an adiabatic condition η (in percentage) (22) and the deviation from isothermal condition, which is defined as the portion of the bridge length with temperatures less than 95% of the maximum temperature (found at the center of the bridge).

where

$$Fo_z = \frac{\alpha_p t}{(l/2)^2}$$

$$C_n = \frac{\int(-\theta_{ss})\sin(\beta_n z)dz}{l/2}$$

$$\beta_n = \frac{n\pi}{l}, \quad n = 1, 2, 3, \ldots. \quad (20)$$

If heat losses by radiation and conduction through the surrounding gasses become significant, the following modifications are required:

$$m^2 = \delta\alpha_{\mathrm{er}} - \frac{h_{\mathrm{conv,bottom}} + h_{\mathrm{conv,top}} + 2h_{\mathrm{rad}}}{kb}$$

$$h_{\mathrm{rad}} \approx 4\varepsilon\sigma T_\infty^3. \quad (21)$$

Adiabatic and isothermal conditions are the most critical concerns in DSC thermal design. If adequately satisfied, these conditions allow the bridge to be considered as a lumped system, and (1)–(3) can be applied to extract the thermophysical properties of specific heat and/or enthalpy. Otherwise, data analysis becomes far more complicated, and the uncertainty in the analysis becomes difficult to estimate. Fig. 5 shows the predicted deviation from adiabatic and isothermal conditions in the proposed suspended bridge structure as a function of time. The deviation from an adiabatic condition is defined as the ratio of heat loss by conduction to the surrounding substrate to the imposed electrical power

$$\eta \equiv \frac{2\int_0^t kwb\frac{dT}{dz}|_{z=l}\,dt'}{Pt}. \quad (22)$$

The assumption of fixed temperature at the base of the bridge, (11), is verified by numerical, analytical, and infrared thermometry, which indicates that the temperature rise at the

base (< 0.1 K) is nearly two orders of magnitude smaller than the typical maximum temperature rise at the center of the bridge (~ 10 K). In addition, there might be a concern regarding the accuracy of the boundary condition described by (11) and the actual boundary condition prevailed in the vicinity of the suspended membrane where the voltage probe is positioned somewhat away from the base of the suspended bridge. It can be shown that the thermal resistance from the voltage probe–bridge intersection to the substrate along the voltage probe is about 50 times larger than the thermal resistance between the voltage probe–bridge intersection and the base of the suspended bridge [Fig. 4(h)], which indicates that the boundary condition represented by (11) prevails.

The deviation from the isothermal condition is defined as the portion of the bridge length with temperatures less than 95% of the maximum temperature (found at the center of the bridge). The typical time constant τ in Fig. 5 is defined as $l^2/\alpha_p\pi^2$, where, at a time equal to one time constant of the system, the first exponential term in the series presented in (19) equals e^{-1}. Using $k_{\text{eff}} = 1$ W/cm-K, $c_{\text{eff}} = 3.43$ J/cm^3-K, and $l = 200$ μm, τ is calculated to be 139 μs.

For example, it can be seen from Fig. 5 that at 1% of the typical time constant (i.e., $t/\tau = 0.01$), the deviation from a perfect adiabatic condition is 5.5%, and the deviation from a perfect isothermal condition is 10%. For typical experimental parameters, the longitudinal Fo_z number at this stage is in the range of 0.1–1. It is noted that a typical duration of experiment using the new setup is on the order of 10 μs, while a typical duration of experiment using the previously reported setups is on the order of 10 ms. When the deviation from isothermal and adiabatic conditions is sufficiently small, only then will the specific heat of the bridge be approximated as the ratio of imposed power to the resulting elevation in temperature.

Note that due to the 1-D nature of the heat transfer process in the new DSC setup, such a quantitative analysis is feasible. Analysis of the previous setups requires 2-D analyses, where a closed-form solution, such as the one presented by (10)–(21), is not available.

B. Data Analysis in the Frequency Domain

The so-called 3ω method is used for data analysis in the frequency domain, which has already been used extensively for the thermal characterization of thin films [18]–[21]. Following the procedure described in [20], expressions for the amplitude and phase delay of temperature in a suspended bridge subjected to a periodic Joule heating are obtained. This method is based on imposing an ac current on the bridge with an angular modulation frequency of ω

$$I_\omega(t) = I \exp(i\omega t). \qquad (23)$$

As a result, Joule heating is generated in the bridge, which causes temperature variation in an angular frequency of 2ω

$$q(t) = \frac{I^2 R_0}{wbl}(1 + e^{2i\omega t}). \qquad (24)$$

Following similar arguments to those presented for the time-domain data analysis, the heat balance equation in the bridge is

$$k_{\text{eff}}\frac{\partial^2 T}{\partial z^2} + q(t) = c_{\text{eff}}\frac{\partial T}{\partial t} \qquad (25)$$

with the same boundary condition presented in (11). The effective specific heat c_{eff} [Jm^{-3} K^{-1}] and thermal conductivity k_{eff} [Wm^{-1} K^{-1}] of the suspended bridge are given by

$$k_{\text{eff}} = \frac{\sum k_i w_i b_i}{\sum w_i b_i} \qquad (25a)$$

$$c_{\text{eff}} = \frac{\sum c_i w_i b_i}{\sum w_i b_i} \qquad (25b)$$

where c_i and k_i represent the heat capacitance and the thermal conductance of the bridge's constituent layers.

The solution of (25) with the boundary condition presented in (11) is

$$T(z,t) - T_0 = \frac{I^2 R_0}{2wblk_{\text{eff}}\kappa^2}\left(1 - \frac{\cosh(\kappa z)}{\cosh(\kappa l/2)}\right)e^{i2\omega t}$$

$$\kappa^2 = \frac{2\omega i}{k_{\text{eff}}/c_{\text{eff}}}. \qquad (26)$$

For small temperature changes, the voltage difference across the bridge is given by

$$V(t) = R_0\left[1 + \alpha_{\text{er}}\left(\overline{\text{Re}\left[T(z,t)\right]} - T_0\right)\right]I_\omega(t) \qquad (27)$$

where $\overline{\text{Re}[T(z,t)]}$ is the spatial average of the real temperature along the suspended bridge, the phase difference is

$$\Phi(\omega) = \arg\left\{\frac{1}{\kappa^2}\left[1 - \frac{\tanh(\kappa l/2)}{\kappa l/2}\right]\right\} \qquad (28)$$

and a voltage response in an angular frequency of 3ω is

$$V_{3\omega} = \left|\frac{I^3 R_0^2 \alpha_{\text{er}}}{2wblk_{\text{eff}}\kappa^2}\left(1 - \frac{\tanh(\kappa l/2)}{\kappa l/2}\right)\right|. \qquad (29)$$

The equivalent thermal conductivity k_{eff} and specific heat c_{eff} are searched by using two-parameter least-square fitting to obtain the best fit between calculated values of $V_{3\omega}$, (29), and the corresponding experimental results. The frequency-dependent phase is also applied in curve fitting of the equivalent thermal conductivity to verify the 3ω setup. Another verification is the equivalent thermal conductivity k_{eff} by using the steady-state measurement, which is different by nearly 2% from the value obtained using the frequency-domain technique.

VII. RESULTS AND DISCUSSION

Experiments were performed in a continuous flow cryostat (Janis ST-100) that is capable of reaching a vacuum
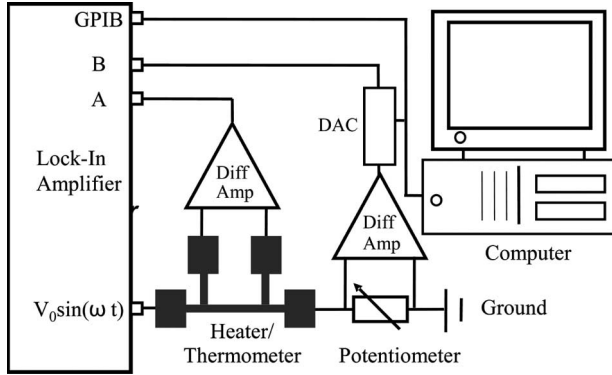
Fig. 6. Schematic illustration of the electrical circuit applied for the 3ω technique of measurement.

(a)

(b)

Fig. 7. Results of specific heat measurements of (a) Cu + SiO$_2$ and (b) Cu + SiO$_2$ + CoFe.

level of 5×10^{-4} torr. All experiments were conducted at room temperature, while the cryostat chamber was used to generate vacuum conditions only. The sample dies were placed on a 68-pin Leadless Chip carrier (LCC), and wires were bonded to provide electrical access to the suspended bridge. The LCC chip carrier was packaged in a socket attached to the copper sample holder. Electrical connections to the socket were made via feed-through channels on the cryostat. A diode temperature sensor (certainty of ± 50 mK) was attached to the sample die to monitor the substrate temperature. Measurements were carried out in two steps: 1) calibration of the TCR for the Cu/SiO$_2$ and Cu/SiO$_2$/CoFe bridges, and 2) differential 3ω measurements to determine the specific heat of the CoFe layer. During the TCR calibration process, a temperature controller was used to keep the base temperature at T_0, and the temperature-dependent resistances of the Cu and Cu/CoFe bridges were recorded, while applying low currents to avoid Joule heating.

Fig. 6 shows schematically the electrical circuit setup used in this study, where the measured parameter is the 3ω voltage component across the sample bridge as a function of frequency ω. The voltage across the sample bridge is measured with the A input of the lock-in amplifier after it passes through a unit gain differential amplifier. The voltage across the potentiometer is measured using the B input of the lock-in amplifier also after it passes through a unit gain amplifier. In addition, a 12-bit digital-to-analog converter (D/A) is used to adjust the output of A to B in order to cancel the large ω component in the circuit and thereby to measure the 3ω component [17]. The lock-in amplifier used in this particular setup had a minimum measurable voltage of 2 nV and a minimum measurable phase shift of $0.01°$.

The experimental work included two steps: 1) TCR calibration of the bridges, and 2) specific heat measurements of the CoFe layer. Data logging was automated by means of a C++ program to control the D/A, the temperature controller, and the lock-in amplifier. Fig. 7 shows experimental results for the reference bridge (Cu/SiO$_2$) and the sample bridge (Cu/SiO$_2$/CoFe). As illustrated in Fig. 7, the reference bridge consists of a 144-nm-thick Cu layer and a 100-nm-thick SiO$_2$ layer, while the sample bridge includes an additional 144-nm CoFe layer, under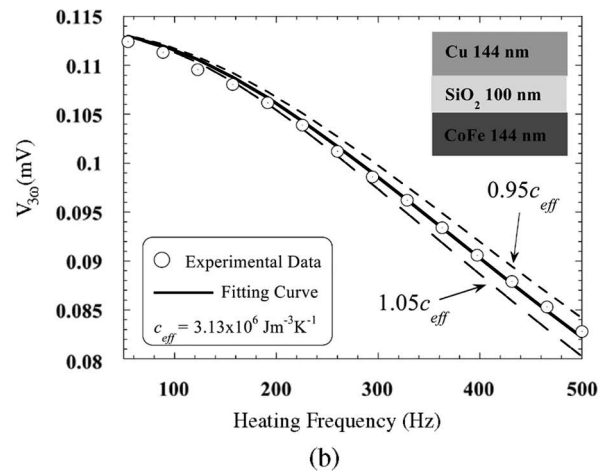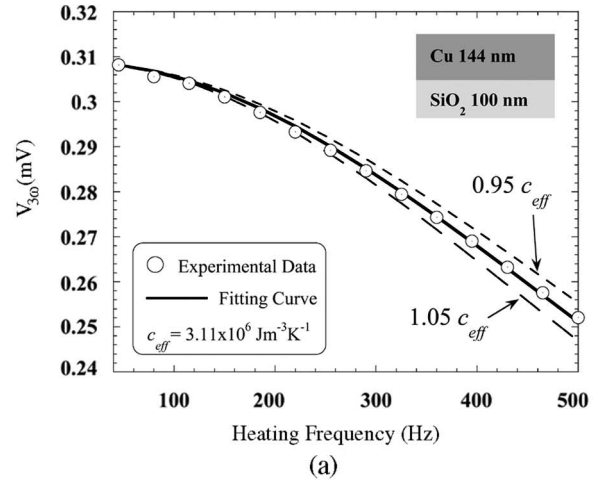 the SiO$_2$ layer. The two bridges have an identical length of 200 μm and width of 15 μm (Fig. 4). The effective specific heat for the reference bridge and the sample bridge were found to be 3.11×10^6 and 3.13×10^6 Jm^{-3} K^{-1}, respectively. The specific heat of the SiO$_2$ layer is calculated to be 2.2×10^6 Jm^{-3} K^{-1} when using a bulk value of 3.43×10^6 Jm^{-3} K^{-1} for the specific heat of the Cu layer and when assuming that the specific heat does not vary significantly between bulk specimens and thin films. Compared with the literature value of 2.0×10^6 Jm^{-3} K^{-1} [23], the results show a very good agreement between the bulk specific heat and the specific heat of a thin layer of SiO$_2$. This level of agreement validates the experimental setup and the technique of measurement. The heat capacity per unit volume of the CoFe layer can be estimated using

$$c_{\text{CoFe}} = \frac{c_{\text{eff},s} \times V_s - c_{\text{eff},r} \times V_r}{b_{\text{CoFe}} \times L \times w} \qquad (30)$$

where V_r and V_s are the volumes of the reference and sample structures, respectively, and b_{CoFe} is the thickness of the CoFe layer. In order to verify the measurement technique, a single CoFe suspended structure with the same dimension as the specimen in the sample bridge was fabricated and measured separately. Equation (30) yields a specific heat value of 3.16×10^6 Jm^{-3} K^{-1} compared to that of a 144-nm-thick single CoFe

suspended structure with $\sim 3.5 \times 10^6$ Jm^{-3} K^{-1} measured independently in this paper. This is about 10% different from the value obtained using differential measurements, which further validates the current experimental structure and measurement technique.

The uncertainty in the 3ω measurement for a single bridge is estimated to be around 5%, which is mainly affected by the uncertainty of the TCR conversion, the width of the bridge, and the thickness of the Cu and CoFe layers. The dashed lines in Fig. 7(a) and (b) represent $\pm 5\%$ variation of the calculated specific heat value. For the differential measurements, the total uncertainty in the specific heat calculation of the CoFe layer is estimated to be 7% (the square root of the sum of the square uncertainties), assuming similar uncertainty for the reference bridge and the sample bridge. The diameter of the data circles in Fig. 7 reflects the sensitivity of the measurement. For example, the diameter of the data circles shown in Fig. 7 represents a $V_{3\omega}$ output of 2 μV, which corresponds to the temperature rise of 80 mK and to an energy change of 0.7 nJ (the product of the minimum detectable elevated temperature, the volumetric specific heat, and the volume of the bridge). The smaller detectable temperature rise corresponds to higher sensitivity. The minimum measurable voltage by the Model SR830 DSP lock-in amplifier is 2 nV, which corresponds to the temperature rise of less than 1 mK and to an energy change of about 1 pJ. It is unlikely that such a high sensitivity can be achieved at room temperature since various sources of noise and uncertainties are likely to limit the detectable energy to nearly 50 pJ.

VIII. Summary and Conclusion

Although small-scale DSC setups have been available for nearly a decade, the thermal analysis presented in the current report suggests that thermal design of previously reported DSC setups may have been over simplified. In those reports, the thermal mass of the substrate was neglected, which leads to an oversimplification of the thermal design and dramatically affecting measurement accuracy and sensitivity. Furthermore, it is speculated that the oversimplified thermal analysis, which targets only heat loss to the substrate and the surroundings, is one of the main sources for inconsistencies in previously reported data.

In this paper, a more detailed thermal analysis of the previously presented small-scale calorimetric setup is presented. This analysis demonstrates the motivation in developing an improved calorimetric technique for small-scale DSC studies. Next, a new setup for small-scale calorimetry is presented based on a suspended bridge configuration. The new technique is based on data analyses in both time and frequency domains. Finally, a validation testing on SiO$_2$ and CoFe is presented.

It is demonstrated that the new setup of a suspended bridge has three major advantages over the prior art: 1) superior temperature uniformity in the bridge cross section; 2) lower heat loss to the surrounding by at least two orders of magnitude; and, 3) fast transient response with heating rate of up to 3×10^6 °C/s. It is shown that certainty in data analysis degrades dramatically when neglecting heat losses to the surroundings,

nonuniformities in temperature distribution, and the coupled thermal effect of the bridge and the substrate.

Experimental validation of the new setup is presented by measuring the specific heat of SiO$_2$ and CoFe layers. The specific heat of the SiO$_2$ layer was found to be 2.2×10^6 Jm^{-3} K^{-1} in comparison with a literature value of 2.0×10^6 Jm^{-3} K^{-1}, which yields a 10% difference. However, the literature value is for bulk specimens, and it may be that the specific heat of thin layers deviates somewhat from that of bulk specimens. The specific heat of the CoFe layer was found to be 3.16×10^6 Jm^{-3} K^{-1} using differential scanning methods compared to the reported value of 3.5×10^6 Jm^{-3} K^{-1} obtained using a single-bridge CoFe structure of the same dimension.

The uncertainty in the 3ω measurement technique for a single bridge is at around 5%, which is mainly affected by the uncertainty of the TCR conversion, the width of the bridge, and the thickness of the Cu and CoFe layers. For the differential measurement, the total uncertainty in the specific heat calculation of the CoFe layer is estimated at 7%, assuming the same uncertainty for the reference bridge and the sample bridge. The minimum detectable energy changes in the new DSC setup is reported to be about 1 nJ, but it is likely that a certainty level on the order of 50 pJ is achievable using the current structure and instrumentations.

References

[1] K. Barmak, J. Kim, S. Shell, E. B. Svedberg, and J. K. Howard, "Calorimetric studies of the A1 to L1$_0$ transformation in FePt and CoPt thin films," *Appl. Phys. Lett.*, vol. 80, no. 22, pp. 4268–4270, Jun. 2002.

[2] S. L. Zhang and M. Oestling, "Metal silicides in CMOS technology: Past, present and future trends," *Crit. Rev. Solid State Mater. Sci.*, vol. 28, no. 1, pp. 1–129, Jan. 2003.

[3] D. Weller, A. Moser, L. Folks, M. Best, W. Lee, M. Toney, M. Schwickert, J. Thiele, and M. Doerner, "High K_u materials approach to 100 Gbits/in^2," *IEEE Trans. Magn.*, vol. 36, no. 1, pp. 10–16, Jan. 2000.

[4] S. L. Lai, J. Y. Guo, V. Petrova, G. Ramanath, and L. H. Allen, "Size-dependent melting properties of small tin particles: Nanocalorimetric measurements," *Phys. Rev. Lett.*, vol. 77, no. 1, pp. 99–102, Jul. 1996.

[5] M. Zhang, M. Y. Efremov, F. Schiettekatte, E. A. Olson, A. T. Kwan, S. L. Lai, T. Wisleder, J. E. Greene, and L. H. Allen, "Size-dependent melting point depression of nanostructures: Nanocalorimetric measurements," *Phys. Rev. B, Condens. Matter*, vol. 62, no. 15, pp. 10 548–10 556, Oct. 2000.

[6] M. Zhang, M. Y. Efremov, E. A. Olson, Z. S. Zhang, and L. H. Allen, "Real-time heat capacity measurement during thin-film deposition by scanning nanocalorimetry," *Appl. Phys. Lett.*, vol. 81, no. 20, pp. 3801–3803, Nov. 2002.

[7] E. A. Olson, M. Y. Efremov, A. T. Kwan, S. Lai, V. Petrova, F. Schiettekatte, J. T. Warren, M. Zhang, and L. H. Allen, "Scanning calorimeter for nanoliter-scale liquid samples," *Appl. Phys. Lett.*, vol. 77, no. 17, pp. 2671–2673, Oct. 2000.

[8] E. A. Olson, M. Y. Efremov, M. Zhang, Z. Zhang, and L. H. Allen, "The design and operation of a MEMS differential scanning nanocalorimeter for high-speed heat capacity measurements of ultrathin films," *J. Microelectromech. Syst.*, vol. 12, no. 3, pp. 355–363, Jun. 2003.

[9] M. Y. Efremov, E. A. Olson, M. Zhang, F. Schiettekatte, and Z. Zhang, "Ultrasensitive, fast, thin-film differential scanning calorimeter," *Rev. Sci. Instrum.*, vol. 75, no. 1, pp. 179–191, Jan. 2004.

[10] F. Hellman, E. N. Abarra, and A. L. Shapiro, "Specific heat of amorphous rare-earth-transition-metal films," *Phys. Rev. B, Condens. Matter*, vol. 58, no. 9, pp. 5672–5683, Sep. 1998.

[11] K. Allen and F. Hellman, "Specific heat of endohedral and higher fullerene thin films," *J. Chem. Phys.*, vol. 111, no. 12, pp. 5291–5294, Sep. 1999.

[12] S. L. Lai, G. Ramanath, and L. H. Allen, "High-speed (10^4 °C/s) scanning microcalorimetry with monolayer sensitivity (J/m^2)," *Appl. Phys. Lett.*, vol. 67, no. 9, pp. 1229–1231, Aug. 1995.

[13] S. L. Lai, G. Ramanath, and L. H. Allen, "Heat capacity measurements of Sn nanostructures using a thin-film differential scanning calorimeter with 0.2 nJ sensitivity," *Appl. Phys. Lett.*, vol. 70, no. 1, pp. 43–45, Jan. 1997.

[14] H. S. Carslaw and J. C. Jaeger, *Conduction of Heat In Solids*, 2nd ed. New York: Oxford Univ. Press, 1986.

[15] X. Zhang and C. P. Grigouopoulos, "Thermal conductivity and diffusivity of free-standing silicon nitride thin films," *Rev. Sci. Instrum.*, vol. 66, no. 2, pp. 1115–1120, Feb. 1995.

[16] W. G. Vincenti and G. H. Kruger, *Introduction to Physical Gas Dynamics*. Melbourne, FL: Krieger, 1965.

[17] Y. C. Tai, C. H. Mastrangelo, and R. S. Muller, "Thermal conductivity of heavily doped low-pressure chemical vapor deposited polycrystalline silicon films," *J. Appl. Phys.*, vol. 63, no. 5, pp. 1442–1447, Mar. 1988.

[18] D. G. Cahill, "Thermal conductivity measurement from 30 to 750 K: The 3ω method," *Rev. Sci. Instrum.*, vol. 61, no. 2, pp. 802–808, Feb. 1989.

[19] L. Lu, W. Yi, and D. L. Zhang, "3ω method for specific heat and thermal conductivity measurements," *Rev. Sci. Instrum.*, vol. 72, no. 7, pp. 2996–3003, Jul. 2001.

[20] M. V. Arx, O. Paul, and H. Baltes, "Determination of the heat capacity of CMOS layers for optimal CMOS sensor design," *Sens. Actuators A, Phys.*, vol. 46, no. 1, pp. 428–431, Mar. 1995.

[21] M. V. Arx, M. Plattner, O. Paul, and H. Baltes, "Micromachined hot plate test structures to measure the heat capacity of CMOS IC thin films," *Sens. Mater.*, vol. 10, no. 8, pp. 503–517, 1988.

[22] S. Zhang, Y. Yang, S. M. Sadeghipour, and M. Asheghi, "Thermal characterization of the 144 nm GMR layer using microfabricated suspended structures," presented at the ASME Summer Conf. National Heat Transfer Conf., Las Vegas, NV, Jul. 21–23, 2003, Paper HT2003-40270.

[23] J. F. Shackelford and W. Alexander, *CRC Materials Science and Engineering Handbook*, 3rd ed. Boca Raton, FL: CRC, 2001.

Shu Zhang received the B.S. degree in precision instruments from Tsinghua University, Beijing, China, in 1998, the M.S. degree in mechanical engineering from the University of California, Irvine, in 2001, and the Ph.D. degree in mechanical engineering from Carnegie Mellon University, Pittsburgh, PA, in 2006.

He is currently with the Recording Head Group, Seagate Technology, Bloomington, MN. His research interests include the field of microelectromechanical systems (MEMS), with a special interest in nanoscale heater transfer design.

Yoed Rabin received the B.Sc. and M.Sc. degrees in mechanical engineering from Ben-Gurion University, Beer-Sheva, Israel, in 1989 and 1991, respectively, and the D.Sc. degree from Technion, Israel Institute of Technology, Haifa, Israel, in 1994.

In 1994, he became a Faculty Member at the Department of Human Oncology, Allegheny University of the Health Sciences, Pittsburgh, PA. In 1997, he returned to hold a Faculty position in the Department of Mechanical Engineering, Technion. He joined Carnegie Mellon University, Pittsburgh, in 2000, where he got promoted to Professor of Mechanical Engineering since 2006. His research activity in the Biothermal Technology Laboratory, which he heads, is focused on cryosurgery, cryopreservation, hyperthermia, thermal regulation of biological processes, and sensors and instrumentation. He has published more than 140 publications in scientific journals, book chapters, conference proceedings, and patents.
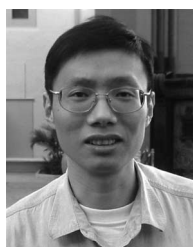
Yizhang Yang received the B.S. and M.S. degrees in engineering mechanics from Tsinghua University, Beijing, China, in 1997 and 2000, respectively, and the Ph.D. degree from Carnegie Mellon University, Pittsburgh, PA, in 2005.

He is currently with the Recording Head Group, Seagate Technology, Bloomington, MN. His research interests are focused on microscale heat conduction in data storage devices and the development of novel microscale thermal characterization techniques.

Mehdi Asheghi received the Ph.D. degree from Stanford University, Stanford, CA, in 1999.

In 2000, he conducted postdoctoral research in the area of nanoscale thermal engineering of microelectronic devices. From 2000 to 2006, he led a well-known and funded research program at the Department of Mechanical Engineering, Carnegie Mellon University, Pittsburgh, PA, that focused on addressing the thermal challenges facing the semiconductor and data storage industries. He is currently with iCONA Technology, Palo Alto, CA—a research and development firm focusing on smart energy and thermal management of data centers and microprocessors. He is the author of more that 120 book chapters, journal publications, and fully reviewed conference papers.